Passively mode-locked laser with an ultra-narrow spectral width

Article (Accepted Version)

This is the author's accepted version, which may not correspond exactly with the published version.
The version of record may be found at: Nature Photonics - DOI:10.1038/nphoton.2016.271

Please cite as: Michael Kues, Christian Reimer, Benjamin Wetzel, Piotr Roztocki, Brent E. Little, Sai T. Chu, Tobias Hansson, Evgeny A. Viktorov, David J. Moss and Roberto Morandotti, "Passively mode-locked laser with an ultra-narrow spectral width," Nature Photonics, Vol. XX, pp. XX (2017)

Passively mode-locked laser with an ultra-narrow spectral width

Michael Kues,1,* Christian Reimer,1 Benjamin Wetzel,1,2 Piotr Roztocki,1 Brent E. Little,3 Sai T. Chu,4 Tobias Hansson,1 Evgeny A. Viktorov,5 David J. Moss,6 and Roberto Morandotti1,7,*

1INRS-EMT, 1650 Boulevard Lionel-Boulet, Varennes, Québec, J3X 1S2, Canada.

2School of Mathematical and Physical Sciences, University of Sussex, Falmer, Brighton BN1 9RH, UK. 3Xi'an Institute of Optics and Precision Mechanics of CAS, Xi'an, China.

4Department of Physics and Material Science, City University of Hong Kong, Tat Chee Avenue, Hong Kong, China.

5National Research University of Information Technologies, Mechanics and Optics, St. Petersburg, Russia.

6Centre for Micro Photonics, Swinburne University of Technology, Hawthorn, VIC, 3122 Australia.

7Institute of Fundamental and Frontier Sciences, University of Electronic Science and Technology of China, Chengdu 610054, China.

*michael.kues@emt.inrs.ca, *morandotti@emt.inrs.ca

Many different mode-locking techniques have been realized in the past[1,2], yet mainly focusing on increasing the spectral bandwidth to achieve ultra-short, subpicoseconds coherent pulses. In contrast, no mode-locked laser has to date managed to generate Fourierlimited nanosecond pulses featured by the narrow spectral bandwidths required for applications in spectroscopy[3], efficient excitation of molecules[4], sensing, and quantum optics[5]. Here we demonstrate a passively mode-locked laser relying on simultaneous nested-cavity filtering and cavity-enhanced nonlinear interactions within an integrated microring resonator, enabling transform-limited optical pulses in the nanosecond regime (4.3 nanoseconds), with an overall spectral bandwidth of 104.9 MHz – more than two orders of magnitude narrower than previous realizations. The laser ultra-narrow bandwidth allows for the complete characterization of its spectral properties in the

radiofrequency-domain using widely-available, GHz-bandwidth optoelectronic components, in turn revealing the strong coherence of the pulse train.

Over the last few decades, a plethora of methods[1,2,6–15] have been developed to realize numerous pulsed laser systems with performances specially tailored to respond to the needs of various applications. These devices range from Q-switched lasers[6,7] allowing high pulse intensities at low repetition rates with high noise figures utilized for, e.g., material processing[8], to passively modelocked laser systems[1,9–11] enabling the generation of highly stable frequency combs for radiofrequency (RF) synthesis[12] and metrology[16], as well as intense ultra-short attosecond pulses for the study of strong-intensity light-matter interactions such as higher-order nonlinear effects in gases and plasmas[17]. Simultaneously, many advances have been made to realize smaller, energy efficient and less complex laser systems[18]. These have relied on developing innovative modelocking techniques and devices, such as semiconductor saturable absorber mirrors[13,14,19], nonlinear-polarization rotation[10] or nonlinear amplifying loop mirrors (NALM)[15,20,21]. Such innovations have allowed to realize compact mode-locked fiber lasers, which are now increasingly replaceing the previous bulky solid-state pulsed sources.

While many schemes for generating a stable coherent train of "ultra-short" laser pulses are nowadays available, they provide only limited success in generating stable nanosecond (ns) pulses. By using volatile Q-switched operation in dye-[22] and fiber-based lasers[23] or external electro-optic modulation of single-frequency fiber[23] and diode lasers[24,25], nearly transform limited ns pulses have been achieved with flexible pulse durations and repetition rates. However, such schemes are usually associated with significant experimental complexity and cost, and more importantly, typically produce outputs with high noise figures (timing-jitter, etc.) or no pulse-topulse coherence. Trying to take advantage of the typically superior noise characteristics of passive mode-locking techniques, graphene-based saturable absorbers have been used for passive mode-locking[2] of ns pulses. Yet, these systems produce strongly frequency-modulated (i.e. chirped) pulses with the narrowest bandwidths achieved to date in the 10's of GHz range[14,26,27]. Until now, *there has been no mode-locking scheme* that allows for the stable generation of *Fourier-transform limited ns-long laser pulses* with a corresponding spectral bandwidth

in the MHz regime. This limitation is mainly caused by the adverse operation timescales of saturable absorbers, as well as by the low strength of the nonlinear effects typically reachable through nspulses with manageable energies.

Recently, enormous progress has been made to realize optical high quality nonlinear micro cavities whose special optical characteristics enabled, e.g., the realization of stabilized Kerr frequency combs[28]. Here, we make use of these advancements in nonlinear micro cavities to overcome the previously-stated limitations and demonstrate a novel, passively mode-locked laser that allows for *the direct generation of Fourier-transform limited nanosecond optical pulses*, which is also compact and operates with low power-consumption.

We exploited a polarization-maintaining figure-eight NALM laser architecture[15,20] as shown in Figure 1, consisting of a NALM section and an amplification stage. In the NALM section, clockwise propagating light is first amplified (via a semiconductor optical amplifier, SOA) before entering the nonlinear element (in our case an integrated microring resonator – see Methods), while the counter-clockwise propagating light passes through the nonlinear element before being amplified. The intensity-dependent nonlinear phase shift difference between the two inputs of the 50:50 beam splitter (50:50 splitter in Figure 1) enables the light splitting ratio to be controlled by the intensity. Such a NALM mimics the behavior of a saturable absorber and has therefore been widely used for passive mode-locking[2,19]. To provide the required gain for laser operation, we introduced an amplification stage including an Erbium-doped fiber amplifier (EDFA) along with an isolator and a 90:10 output coupler.

In the past, a large variety of *non-resonant* nonlinear elements have been used within the NALM section in order to obtain the required nonlinear phase-shift for mode-locking operation. The novelty of our method relies on the implementation of a *resonant* nonlinear medium that acts as an ultra-narrowband spectral filter, while providing large field enhancement. This configuration enables, in turn, sufficient nonlinear phase-shifts for low-power narrow-bandwidth passive modelocking. Specifically, we used a high-Q microring resonator fabricated in a CMOS-compatible high refractive index silica-based glass[29] with a measured Q-factor of 1,300,000, a free spectral range (FSR) of 200 GHz and an associated resonance bandwidth of around 150 MHz. Additional 200 GHz bandpass filters centered at 1556 nm

were used to select a specific ring resonance. When turning on and increasing the amplifiers' driving currents, the laser first entered a selfstarting single-pulse lasing operation regime, whereas at higher driving currents the laser exhibited complex dynamics including multi-stability, soliton bunching or even chaotic pulsing

30.

In the stable pulsed regime (on which we focus here), the laser emitted a pulse train with a f_R =9.565 MHz repetition rate (Figure 2a), exhibiting excellent stability as confirmed by RF spectral measurements (Figure 2c) and showing, at the same time, negligible modulation components below -35 dB. The pulse temporal profile (Figure 2b) is well described by a Gaussian function $|E_{P^4}(t)|^2$ (see Methods and solid blue line in Figure 2b) with a duration of 4.31 ns (FWHM) and a low temporal jitter of ±0.13 ns. With an average optical output power of ~2.5 mW, the passive mode-locking of nanosecond pulses was achieved at peak powers as low as ~60 mW. Interestingly, even using intrinsically very noisy amplifiers (SOAs), the pulse train stability was still excellent (< 2.3% RMS).

In contrast to previous reports of mode-locked nanosecond pulsed lasers that were featured by hundred-GHz-wide spectra [14,26,27], the bandwidth of our laser system is in the hundred-MHz range, and thus not accurately resolvable with the resolution and stability of common optical spectrum analyzers, nor measurable with standard pulse characterization techniques (e.g. SPIDER, FROG). At the same time, the spectral width of the laser is compatible with the bandwidth of widely-available photo-detectors and signal-processing electronics (i.e. ~GHz range or less). In this case, the coherent beating between the mode-locked laser field and a stable CW laser field allows us to map the entire optical spectrum into the RF domain. The RF spectrum (in Figure 3a) reveals two prominent parts whose envelope is associated with i) the intensity Fourier transform (FT) of the pulse (lower frequency part – green shading) and ii) the so-called beat note

(higher frequency part – red shading), which relates to the electric field spectrum of the pulse (see Methods). The beat note, centered around 1,600 MHz, allows us to resolve not only the spectral shape

but also the comb-like structure of the mode-locked laser associated with its repetition rate (i.e. each oscillating laser mode corresponds to a different beat frequency).

Figure 3b compares the measured spectral shape (red crosses) with the ideal Fourier-limited spectrum retrieved from the temporal trace (purple dash line), showing small discrepancies in the spectral wings, which can be attributed to a small intensity-dependent temporal phasemodulation, associated with the Kerr effect (blue solid line, see Methods). From this, we retrieved a spectral laser bandwidth of $\Delta\nu_{Kerr\ Cont.}$ = 104.9 MHz, a record-low value for any passively mode-locked laser, and only marginally different from the bandwidth of the non-phasemodulated spectrum ($\Delta\nu$ = 102.3 MHz). For comparison with other characterization techniques, the bandwidth measurement performed with a state-of-the art high-resolution optical spectrum analyzer is presented in Figure 3b (dashed green line), showing only the qualitative trend of the spectral shape (limited by the device measurement uncertainties – see Methods).

The ultra-narrow bandwidth of our laser also permits the retrieval of additional information concerning the mode-locking properties of the system, such as the coherence of the spectral modes. In particular, the intensity FT, related to the lower-frequency part, describes the intermodal beating of each comb mode with the others, once the comb-like frequency distribution is taken into account (see Methods). For previous (large bandwidth) mode-locked lasers, the entire shape of this convolution was not resolvable due to bandwidth limitations of the electronics and photo-detector. However, in our case, the laser characteristics *enable us to resolve the relative contributions of the spectral wings* (i.e. frequencies that are outside the FWHM) to each

RF tone (red crosses in Figure 3c – see Methods). Considering the different contributions to the RF spectrum, we compared the beat note at f_R = 9.565MHz and at $26f_R$ – see inset of Figure 3c. For both cases, the convolution linewidths perfectly matched, allowing us to conclude that the mode linewidths remain equal over the whole comb (within the measurement uncertainties), thus demonstrating the coherent locking of all laser modes.

Finally, our laser scheme is highly flexible in terms of central lasing frequency and bandwidth. By exploiting a micro ring with a resonance bandwidth of 650 MHz (corresponding to a Q-factor of

300,000), we also achieved mode-locking operation with 0.57 ns bandwidth-limited pulses, demonstrating the tunability in pulse width offered by this approach. Moreover, we achieved mode-locked operation at several wavelengths by selecting different resonances with suitable filters. Additional wavelength fine-tuning over the FSR of the resonator was obtained through thermal control with a temperature-frequency dependence of 1.86 GHz/°C, see Figure 4.

With the bandwidth and wavelength fine-tuning capability, the pulsed laser presented here is perfectly suited to excite nonlinear high-Q cavity resonances and narrowband atomic/molecular transitions. In this regard, the beating technique used here allows an easy spectral analysis of the probed sample, providing a practical tool for characterization.

In conclusion, the unique combination of record-narrow spectral bandwidth and resulting high spectral density, along with low power operation and large tunability of the emitted frequency, make this laser very versatile and extremely useful for a large number of applications. The compact architecture, and modest requirements in terms of power, readily allow for stable and portable operation, while opening up a route towards the full integration of the laser system.

Together with the possibility to resolve the full laser spectrum in the RF domain, such characteristics will pave the way towards novel sensing and spectroscopy implementations. From a fundamental perspective, the low and tractable number of modes (11 within the spectral FWHM), may enable further studies of both nonlinear mode coupling and complex mode-locking regimes.

References

1. Ippen, E. P. Principles of Passive Mode Locking. *Appl. Phys. B* **58,** 159–170 (1994).
2. Keller, U. Recent developments in compact ultrafast lasers. *Nature* **424,** 831–838 (2003).
3. Mandon, J., Guelachvili, G. & Picque, N. Fourier transform spectroscopy with a laser frequency comb. *Nat. Phys.* **3,** 99–102 (2009).
4. Wrigge, G., Gerhardt, I., Hwang, J., Zumofen, G. & Sandoghdar, V. Efficient coupling of photons to a single molecule and the observation of its resonance fluorescence. *Nat. Phys.* **4,** 60–66 (2008).
5. Reimer, C. *et al.* Generation of multiphoton entangled quantum states by means of integrated frequency combs. *Science.* **351,** 1176–1180 (2016).
6. McClung, F. J. & Hellwarth, R. W. Giant Optical Pulsations from Ruby. *J. Appl. Phys.* **33,** 828–829 (1962).
7. Wolf, E. *Progress in optics*. (Elsevier, 2004).
8. Steen, William, Mazumder, J. *Laser material processing*. (Springer, 2010).
9. Spence, D. E., Kean, P. N. & Sibbett, W. 60-fsec pulse generation from a self-modelocked Ti : sapphire laser. *Opt. Lett.* **16,** 42–44 (1991).
10. V. J. Matsas, T. P. Newson, D. J. R. and D. N. P. Selfstarting passively mode-locked fibre ring soliton laser exploiting nonlinear polarisation rotation. *Electron. Lett.* **28,** 1391–1393 (1992).
11. Haus, H. A. & Fellow, L. Mode-Locking of Lasers. *IEEE J. Sel. Top. QUANTUM Electron.* **6,** 1173–1185 (2000).
12. Jones, D. J. *et al.* Carrier-Envelope Phase Control of Femtosecond Mode-Locked Lasers and Direct Optical Frequency Synthesis. *Science.* **288,** 635–639 (2000).
13. Sun, Z. *et al.* A Stable, Wideband Tunable, Near Transform-Limited, Graphene-ModeLocked, Ultrafast Laser. *Nano Res.* **3,** 653–660 (2010).
14. Kelleher, E. J. R. *et al.* Nanosecond-pulse fiber lasers mode-locked with nanotubes. *Appl. Phys. Lett.* **95,** 111108 (2010).
15. Richardson, D. J., Laming, R. I., Payne, D. N., Matsas, V. & Phillips, M. W. Selfstarting passively modelocked erbium fibre ring laser based on the amplifying Sagnac switch. *Electron. Lett.* **27,** 542–544 (1991).
16. Udem, T., Reichert, J., Holzwarth, R. & Hänsch, T. W. Absolute Optical Frequency Measurement of the Cesium D1 Line with a Mode-Locked Laser. *Phys. Rev. Lett.* **82,** 3568 (1999).
17. Brabec, T. & Krausz, F. Intense few-cycle laser fields : Frontiers of nonlinear optics. *Rev.*
    Mod. Phys. **72,** 545–591 (2000).
18. Fermann, M. E. & Hartl, I. Ultrafast fibre lasers. *Nat. Photonics* **7,** 868–874 (2013).
19. Keller, U. *et al.* Semiconductor Saturable Absorber Mirrors (SESAM's) for Femtosecond to Nanosecond Pulse Generation in Solid-State Lasers. *IEEE J. Sel. Top. QUANTUM Electron.* **2,** 435–453 (1996).
20. Duling, I. N. Subpicosecond all-fibre erbium laser. *Electron. Lett.* **27,** 544–545 (1991).
21. Zhong, Y. H., Zhang, Z. X. & Tao, X. Y. Passively Mode Locked Fiber Laser Based on Nonlinear Optical Loop Mirror with Semiconductor Optical Amplifier. *Laser Phys.* **20,** 1756–1759 (2010).

22. Bolger, B. & Baede, L. Production of 300W, nanosecond, transform limited optical pulses. *Opt. Commun.* **19,** 346–349 (1976).
23. Shi, W., Leigh, M. A., Zong, J., Yao, Z. & Nguyen, D. T. High-Power All-Fiber-Based Narrow-Linewidth Single-Mode Fiber Laser Pulses in the C-Band and Frequency

Conversion to THz Generation. *IEEE J. Sel. Top. Quantum Electron.* **15,** 377–384 (2009).
24. Nicolaescu, R., Fry, E. S. & Walther, T. Generation of near-Fourier-transform-limited high-energy pulses in a chain of fiber – bulk amplifiers. *Opt. Lett.* **26,** 13–15 (2001).
25. Schorstein, K. & Walther, T. A high spectral brightness Fourier-transform limited nanosecond Yb-doped fiber amplifier. *Appl. Phys. B* **97,** 591–597 (2009).
26. Wang, H. *et al.* All-fiber mode-locked nanosecond laser employing intracavity chirped fiber gratings. *Opt. Express* **18,** 4467–4470 (2010).
27. Xia, H., Li, H., Wang, Z., Chen, Y. & Zhang, X. Nanosecond pulse generation in a graphene mode-locked erbium-doped fiber laser. *Opt. Commun.* **330,** 147–150 (2014).
28. Brasch, V. *et al.* Photonic chip – based optical frequency comb using soliton Cherenkov radiation. *Science.* **351,** 357–360 (2016).
29. Moss, D. J., Morandotti, R., Gaeta, A. L. & Lipson, M. New CMOS-compatible platforms based on silicon nitride and Hydex for nonlinear optics. *Nat. Photonics* **7,** 597–607 (2013).
30. Grelu, P. & Akhmediev, N. Dissipative solitons for mode-locked lasers. *Nat. Photonics* **6,** 84–92 (2012).
31. Stolen, R. H. Optical Kerr effect in glass waveguide. *Appl. Phys. Lett.* **22,** 294 (1973).

Figures

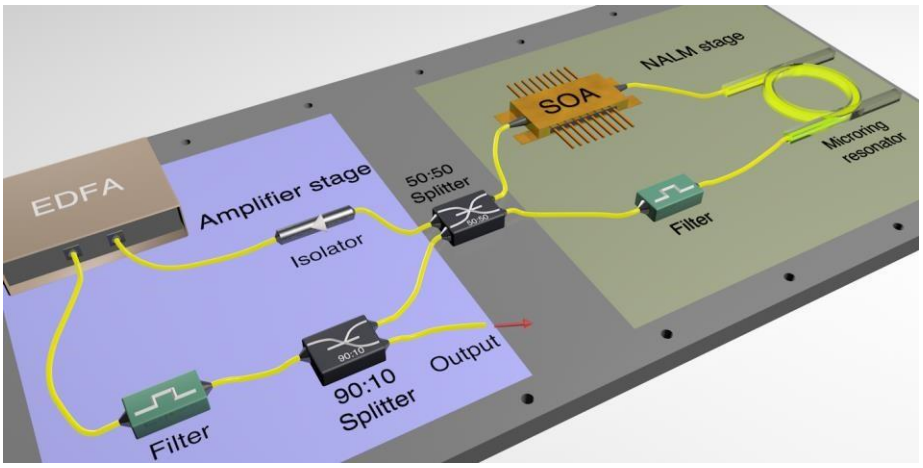

Figure 1 | Experimental setup of the laser scheme. Nonlinear amplifying loop mirror (NALM) stage (right) and an amplifier stage (left), constituting the ns mode-locked laser. The NALM stage consists of the microring resonator (free spectral range 200 GHz, Q-factor 1.3M), a filter (200 GHz at 1556 nm, determining the ring resonance of operation), a semiconductor optical amplifier (SOA), and a 50:50 beam splitter, connecting the NALM to the amplification stage. This section contains an optical isolator (determining the direction of pulse propagation), an erbium-doped fiber amplifier (EDFA), a second filter (200 GHz at 1556 nm), as well as a 90:10 beam splitter for coupling 10% of the power at the output. All elements are optically connected by polarization-maintaining fibres, ensuring an environmentally-stable operation.

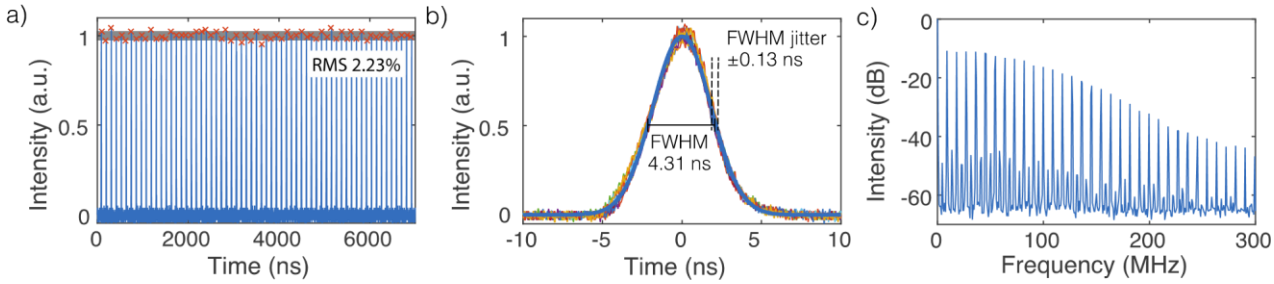

Figure 2 | Laser characterization. a, Real-time time trace of 55 pulses with RMS noise below 2.3 %. **b**, Temporal profile of the emitted pulses (10 pulses superimposed) with a 4.31 ns FWHM Gaussian pulse fit (blue solid line) and a low FWHM jitter of 0.13 ns. **c**, Radio-frequency spectrum of the mode-locked laser output, showing clear and narrow peaks at the repetition rate of the laser (9.565 MHz). In addition, we observe a negligible modulation at -35dB, attributed to back reflections at the waveguide-microring interface from the clockwise and counter-clockwise propagating light. As the resonator is not placed in the center of the NALM, the back-reflected components arrive at different times at the beam splitter. The path-length difference of 4.2 m between the two reflections results in an expected noise beat-note frequency of 23.8 MHz. This value is in good agreement with the frequency component observed at 23.3 MHz in the RF spectrum.

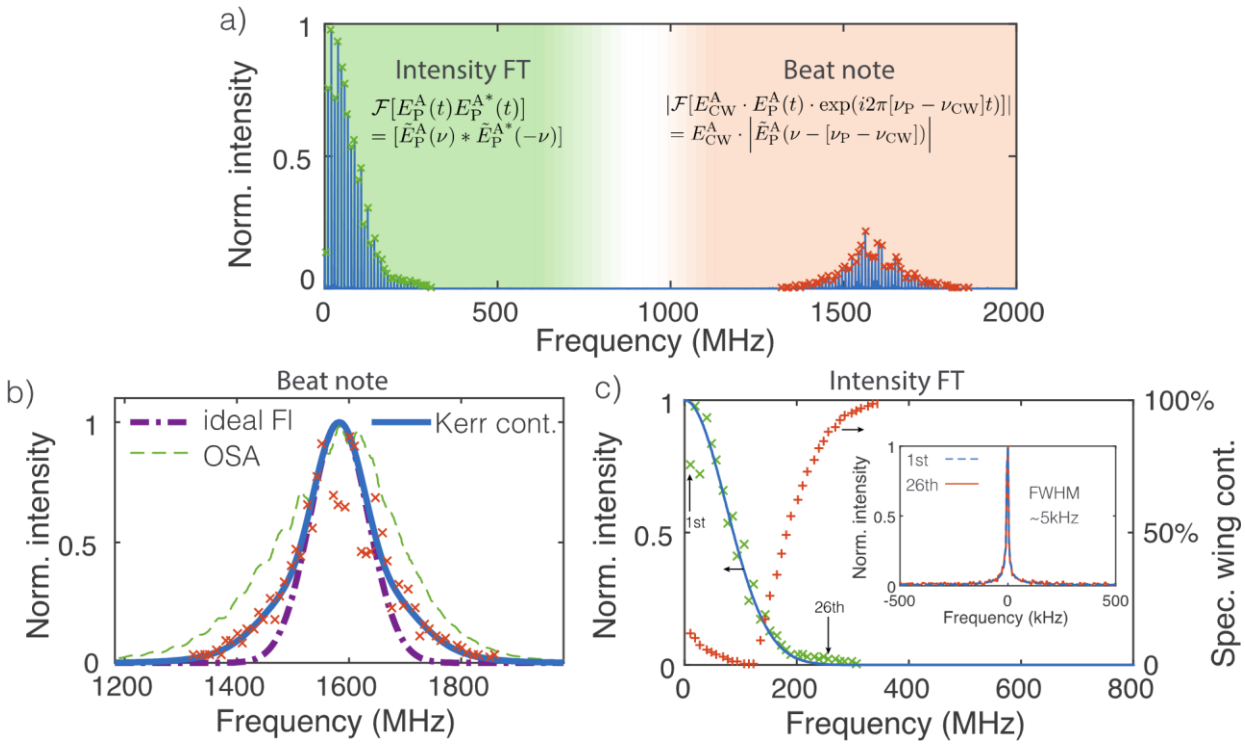

Figure 3 | Beating measurement with a CW laser. a, By beating the nanosecond mode-locked laser with a CW laser, the complete laser spectrum can be mapped into the RF spectrum. The RF spectrum can be divided into the beat note and the intensity Fourier transform (FT) parts, respectively. **b**, Beat note (red crosses), ideal Fourier-limited spectrum obtained from the temporal pulse profile (dash-dotted purple line), spectrum obtained from the temporal pulse profile assuming an additional temporal phase modulation due to the Kerr effect (blue solid line), and high-resolution optical spectrum analyzer measurement (green dashed line). The deviations of the measured beat note (red crosses) from the fit in the central part can be mainly attributed to measurement uncertainties stemming from a small signal-to-noise ratio of the beat signal between pulses (which can be improved through the use of a stronger signal and a low-noise photo detector). **c**, Experimental intensity FT from the beating measurement

(green crosses), in good agreement with the calculated values (blue solid line). The contribution of the spectral wings (that is, the spectral components outside the spectral FWHM) to the RF tone is shown as red crosses. Inset: spectral shape of the 1st RF tone (for which the impact of optical frequencies *within* the spectral FWHM is ~90%) and 26th RF tone (for which, conversely, the impact of optical frequencies *outside* the spectral FWHM is ~90%).

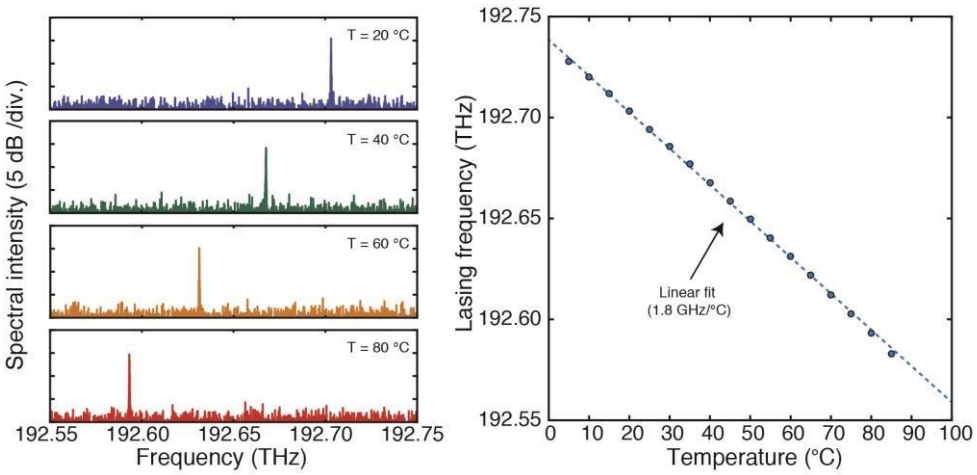

Figure 4 | Temperature tuning characteristics of the laser emission frequency. Temperaturebased fine-tuning of the emission spectra (left panel). A linear relationship between the chip temperature and lasing frequency for stable pulsed operation is measured with a slope of 1.8 GHz/ºC (right panel). This property allows operation of the laser within a large frequency interval by first coarsely selecting a desired resonance through a filter, and then performing a finer temperature adjustment.

Methods

Device: The microring resonator was fabricated using UV photolithography and reactive ion etching in a CMOS-compatible high refractive index silica glass prepared by chemical vapour deposition without the need for high temperature annealing. The used material platform –Hydex– is featured by very low linear (0.06 dB/cm) and negligible nonlinear optical losses (no nonlinear losses measured up to 25 GW/cm^2), and a high effective nonlinearity (γ=233W^{-1}km^{-1}). The microring resonator was vertically coupled to two bus waveguides, forming a four-port configuration. The input and output bus waveguides were featured with mode converters and were pigtailed to polarization maintaining single-mode fibres, resulting in coupling losses of 1.6 dB per facet.

Experimental characterization: The pulse temporal measurements were conducted with a fast photodetector (10 GHz – Lab Buddy DSC-R403), which was connected to a high-bandwidth realtime

oscilloscope (8 GHz – Tektronix DPO 70804). The optical spectrum measurements were performed with a high-resolution optical spectrum analyzer (Apex AP2043B), having measurement uncertainties of ±37.5MHz.

Beating measurement: We used a highly stable CW laser (local oscillator from Apex AP2043B, linewidth <100kHz) and superimposed it through a fiber coupler to the output of the mode-locked laser. The beat note was measured using the fast photodetector connected to the high-bandwidth real-time oscilloscope.

The electric field of the CW laser is defined as: $E_{CW} = E_{CW}{}^{A} \exp(i2\pi\nu_{CW}t) + c.c.$ The field of the mode-locked laser is defined as: $E_P = E_P{}^{A}(t) \exp(i2\pi\nu_P t) + c.c.$ where $E_P{}^{A}(t) =$

t^2 exp $(-(\ ))$ is the electric field temporal pulse shape, which is Gaussian. Here we consider the

T

envelope of one pulse rather than the complete pulse train. For the conducted beating

measurement, the photocurrent is proportional to $P \sim |E_{CW} + E_P|^2 = E_{CW}E_{CW}{}^{*} + E_{CW}E^{*} + E_{CW}{}^{*}\ E_P\ _P + E_P E_P{}^{*}$. Inserting the above defined fields we obtain: $P \sim [E_{CW}{}^{A}\, E_{CW}{}^{A*} + 2 *$ 12

$Re\{E_{CW}{}^{A}\, E_P{}^{A*}(t) \exp(i2\pi[\nu_P - \nu_{CW}]t)\} + E_P{}^{A}(t)E_P{}^{A*}(t)]$ (note that we do not account for the conjugate complex part, as it leads to higher frequency components not detectable within our RF spectral measurements). Applying the Fourier transform to obtain the RF spectrum and omitting the negative frequencies yields: $|\mathcal{F}[P]| \sim [const. + |E_{CW}{}^{A}\, \tilde{E}_P{}^{A}(\nu - (\nu_P - \nu_{CW}))| + \tilde{E}_P{}^{A}(\nu) * \tilde{E}_P{}^{A*}(-\nu)]$. The first term is a constant value emerging from the CW laser beating with itself. The second term describes the beating of the CW laser with the mode-locked laser, $E_{CW}{}^{A}\, |\tilde{E}_P^{A*}(\nu -$

$(\nu_P - \nu_{CW}))|$, thus enabling the measurement of the absolute field spectrum in the RF domain. The third term –the intensity FT– is related to the convolution of the electric field spectrum of the mode-locked laser with its time-reversed complex conjugate (corresponding in our case to the lower frequency part).

RF analysis: Beat note – In Figure 3b, we compare the spectral shape measured from the beat note (red crosses) with the ideal Fourier-limited spectrum (dash-dotted purple line) calculated from the fitted

temporal pulse profile (see Figure 2b), i.e. $\tilde{E}_{P^A} = \mathcal{F}[E_{P^A}(t)]$. It can be observed that the high intensity central part of the Fourier-limited spectrum agrees well with the measured values, however, discrepancies appear on the spectral wings, which are slightly broader for the measured spectrum than for the ideal Fourier-limited case. Although a dispersive pulse broadening effect could be responsible for these discrepancies (i.e. not transform-limited pulse), we estimated that for such a ~100 MHz-bandwidth, dispersive pulse broadening factors originating from the laser elements are of the order of 10^{-6} per meter, and are thus negligible. A more plausible explanation arises from a temporal phase modulation generated through the nonlinear Kerr effect acting within the microring resonator. The blue solid line in Figure 3c shows the calculated spectral profile of the pulse assuming an intensity-dependent phase shift induced by the Kerr effect[31], i.e. $\tilde{E}_{P}{}'^{A} = \mathcal{F}[E_{P^A}(t) \cdot \exp(i \cdot 2\pi \cdot g \cdot |E_{P^A}(t)|^2)]$, with g being a dimensionless factor related to the nonlinear strength. For a fitted g = 0.1273, the resulting spectrum agrees well with the experimental data, especially in the spectral wings. A laser bandwidth of $\Delta\nu'$= 104.9 MHz was retrieved, only marginally different from the bandwidth of the non-phase-modulated spectrum ($\Delta\nu$ = 102.3 MHz). The bandwidth obtained from the OSA measurement $\Delta\nu_{OSA}$ = 145 MHz deviated from the previously measured one – within the OSA measurement uncertainties of ±37.5MHz broadening the spectrum.

Intensity FT – The lower frequency part of the RF beating spectrum (green crosses, see Figure 3c) can be related to the convolution of the pulse electric field spectrum with its inverse complex conjugate $\tilde{E}_{P^A}(\nu) * \tilde{E}_{P^{A*}}(-\nu)$. Taking into account the comb nature of the mode-locked laser, this convolution can be interpreted as the beating of all laser modes with each other (i.e. the first RF tone is the sum of the beat intensities from next neighbouring frequency components, the second RF tone is the sum of beat intensities from second-next neighbouring frequency components, etc.). This implies that higher frequency RF tones have higher contributions from the spectral wings. By numerically calculating this convolution for a comb spectrum that only includes frequencies outside the FWHM (i.e. only counting the modes in the spectral wings) and comparing it with the result for a complete spectrum (i.e. including all frequency modes), we could retrieve the relative contribution of the spectral wings to each RF tone (red crosses in Figure 3b).

Author contributions

M.K. and C.R. developed the idea and the experiment. B.E.L and S.T.C designed and fabricated the integrated device. C.R., M.K., B.W, and P.R., performed the measurements and analyzed the experimental results. E.A.V and T.H. helped with the analysis of the RF measurement technique and the evaluation of the laser performance. R.M. supervised and managed the project. All authors contributed to scientific discussions and the writing of the manuscript.

Acknowledgments

This work was supported by the Natural Sciences and Engineering Research Council of Canada (NSERC) through the Steacie and Discovery Grants Schemes, and by the Australian Research Council Discovery Projects scheme. C.R. and P.R. acknowledge the support of NSERC Vanier Canada Graduate Scholarships. M.K. acknowledges support from FRQNT (Fonds de Recherche du Québec–Nature et Technologies) through the MELS fellowship program (Merit Scholarship Program for Foreign Students; Ministère de l'Éducation, de l'Enseignement Supérieur et de la Recherche du Québec). M.K. also acknowledges funding from the European Union's Horizon 2020 research and innovation program under the Marie Sklodowska-Curie grant agreement no. 656607. We acknowledge the support from the People Programme (Marie Curie Actions) of the European Union's FP7 Programme: B.W. for INCIPIT under REA grant agreement n° [625466]. S.T.C. acknowledges the support from the CityU SRG-Fd program #7004189. We thank Robin Helsten for the design of the temperature controller, José Azaña for providing some of the required experimental equipment, and Guillaume Huyet for useful discussions.